Micropencils and Microhexagonal Cones of ZnO

Niranjan S. Ramgir, Imtiaz S. Mulla, and Vijayamohanan K. Pillai*

Physical and Materials Chemistry Division, National Chemical Laboratory, Pune 411008, India

Received: November 16, 2005; In Final Form: December 29, 2005

Shape selective synthesis of ZnO micropencils and microhexagonal cones has been demonstrated using a controlled method of modified vapor deposition. A plausible growth mechanism based on the results of scanning electron microscopy, X-ray diffraction, X-ray photoelectron spectroscopy, thermogravimetry, and differential thermal analysis is proposed. Our results suggest that growth of micropencil takes place as per the vapor−liquid−solid progression while the microhexagonal cones grow in two steps following a vapor−solid/vapor−liquid−solid mechanism. Moreover, the geometry, the location of substrate and temperature are found to have key roles in governing the morphology. XPS studies clearly demonstrate the presence of Si species as SiO and SiO_2, which act as catalysts enabling nucleating sites for ZnO microstructural growth.

1. Introduction

With the advent of various structures of functional materials namely SnO_2[1], TiO_2[2], WO_3[3], and ZnO,[4] there has been an upsurge in the interest in studying the basic issues about dimensionality and space-confined transport phenomena with respect to their important applications. The shape and size of these structures play crucial roles in controlling their widely varying physical, chemical, and electronic properties. Among these, ZnO, a wide band gap semiconducting oxide material (3.2 eV) possessing excellent chemical and thermal properties, with a large exciton binding energy (60 meV) can realize practical applications in the area of chemical sensors, nanoscale laser diodes, and field emission devices.[5] Accordingly, it has been synthesized in different forms namely tetrapods,[6] nanowires,[7] nanotubes,[8] nanosprings,[9] etc. using several methods, such as pyrolysis, chemical treatment, template, heat treatment, and so on. Of the various methods adopted, the thermal vapor method is a commonly exploited one as it offers the advantage of low reaction time below 1 h. Moreover, the precise control over the geometry of the materials can be achieved by a simple ascendancy of the preparation parameters, namely temperature, duration of heating, nature of the substrate, type of carrier gas, and oxygen flow rate. Usually, the nanostructures grow via a self-catalytic process in which the precision, prediction, and reproducibility, all emerge from the nature of interactions between the constituent elements. Our group has recently elucidated a refined, plausible growth mechanism for different morphologies of SnO_2 using a simple process of vapor deposition.[10]

Here, we demonstrate the shape-selective synthesis of novel ZnO microstructures, namely micropencils and microhexagonal cones, using a simple approach of modified vapor deposition. We discuss the plausible growth mechanism based on the results of scanning electron microscopy, X-ray diffraction, X-ray photoelectron spectroscopy, and thermogravimetric analysis. Our studies indicate that growth of a micropencil takes place as per the vapor−liquid−solid progression, while the microhexagonal cones grow in two steps following a vapor−solid/ vapor−liquid−solid mechanism.

2. Experimental Section

(a) Synthesis of Micropencils and Microhexagonal Cones. Scheme 1 shows the experimental setup used for the synthesis of ZnO structures. Pure Zn metal, (melting point = 420 °C, boiling point = 907 °C) was heated at a temperature of 950°C for 2 h in a mixed environment of argon and oxygen flowing at a rate of 100 ± 5 and 20 sccm (20% v/v) respectively, on an alumina substrate, kept on a commercially available aluminosilicate refractory brick substrate. The pencils were found to grow on the aluminosilicate substrate, while hexagonal cones were formed on the opposite side of the substrate kept downstream, where the temperature was between 200 and 500 °C.

(b) Structural and Morphological Characterization. The structure and the morphology were characterized using a scanning electron microscope equipped with energy-dispersive X-ray analysis attachment (A Lieca Stereoscan 440 model SEM with a Kevex model EDX system), X-ray diffractometer (XRD, Philips 1730 machine), and a transmission electron microscope (Philips CM200 FEG microscope). X-ray photoelectron spectroscopic (XPS) measurements were carried out on a VG MicroTech ESCA 3000 instrument at a pressure of $>1 \times 10^{-9}$ Torr (pass energy of 50 eV, electron takeoff angle 60°, and overall resolution ~1 eV). The spectra were fitted using a combined polynomial and Shirley type background function. TG-DTA was carried out in the temperature range 50−900 °C under Ar flow at a heating rate of 5 °C/min on a Perkin-Elmer thermal analyzer.

3. Results and Discussion

(a) Morphological and Structural Characterization. Figure 1 shows the SEM images of the micropencil structures. As can be seen (Figure 1a) the substrate is uniformly coated with ZnO micropencils throughout its surface, suggesting the high density of the freshly grown micropencils. Figure 1b shows the EDX of the micropencil exhibiting a strong signal corresponding to Zn and O. The intensity ratios among the Zn, O and Si peaks

* Corresponding author. Fax: +91-020-25893044; Tel: +91-020-2590 2276. E-mail: vk.pillai@ncl.res.in.

10.1021/jp056629b CCC: $33.50
Published on Web 02/10/2006

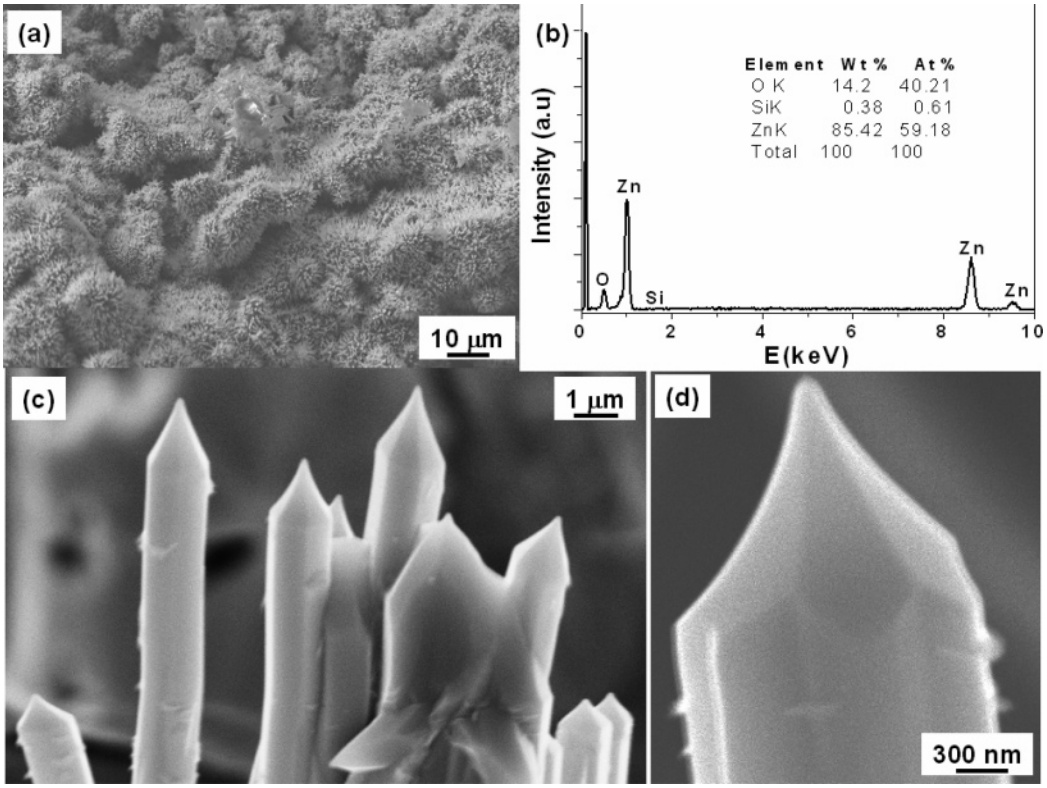

Figure 1. SEM images of the micropencil structure grown on aluminosilicate refractory brick substrate: (a) EDX of the micropencils exhibiting a strong signal corresponding to Zn and O, (b) the enlarged SEMs of the micropencils (c) and (d).

SCHEME 1: Experimental Setup Used for the Synthesis of ZnO Micropencils and Microhexagonal Cones

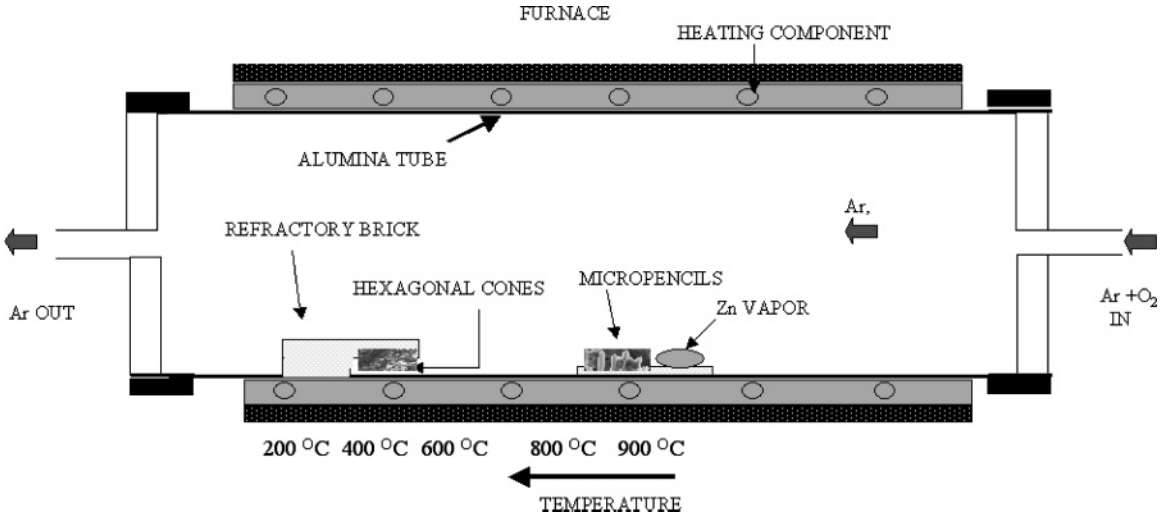

suggest that the Si content in the micropencils is approximately 0.61 at. %. Figures 1c and 1d show slightly enlarged images of the micropencil revealing its clear features. It is observed that the micropencils have a hexagonal shank, with width varying between 800 and 1200 nm, and the shank terminates with a tapering end whose diameter is less than 100 nm. The tapering tip interestingly extends to a length of 300 to 600 nm, with a tip apex of less than 100 nm.

Figure 2 shows the SEM images of the "as-grown" ZnO microhexagonal cones; the hexagonal structures emerge from the surface of the substrate. Indeed, the structure resembles an upside down cone ending into a hexagonal disk. The hexagonal cones are poly dispersed in nature with a size varying from 1 to 80 μm (Figure 2b); the number of edges to all structures is fixed to six. Moreover, the edge length varies randomly from 3 to 20 μm. The six side surfaces and the base of the hexagonal cones appear smooth with a small depression at the center. Figure 2d shows the EDX recorded for hexagonal cones. The intensity ratio among the Zn, O, and Si peaks suggests that the Si content in the microhexagonal cones is approximately 9.11 at. %.

Wurtzite zinc oxide has a hexagonal structure (space-group *C6mc*) with lattice parameters $a = 3.2496$ and $c = 5.2065$ Å (JCPDS Card No. 36-1451). The XRD patterns of the (a) commercial ZnO (Aldrich 99.99% pure), (b) micropencils, and (c) microhexagonal cone structures are shown in Figure 3. The peaks match well with those of commercial ZnO; however, the peak positions shifted toward higher 2θ values attributed, perhaps, to the incorporation of Si species into the ZnO matrix. The intensity of the peaks also differs from that of the bulk due to the larger number of planes along the long axis of the structures as compared to that along the diameter.[11]

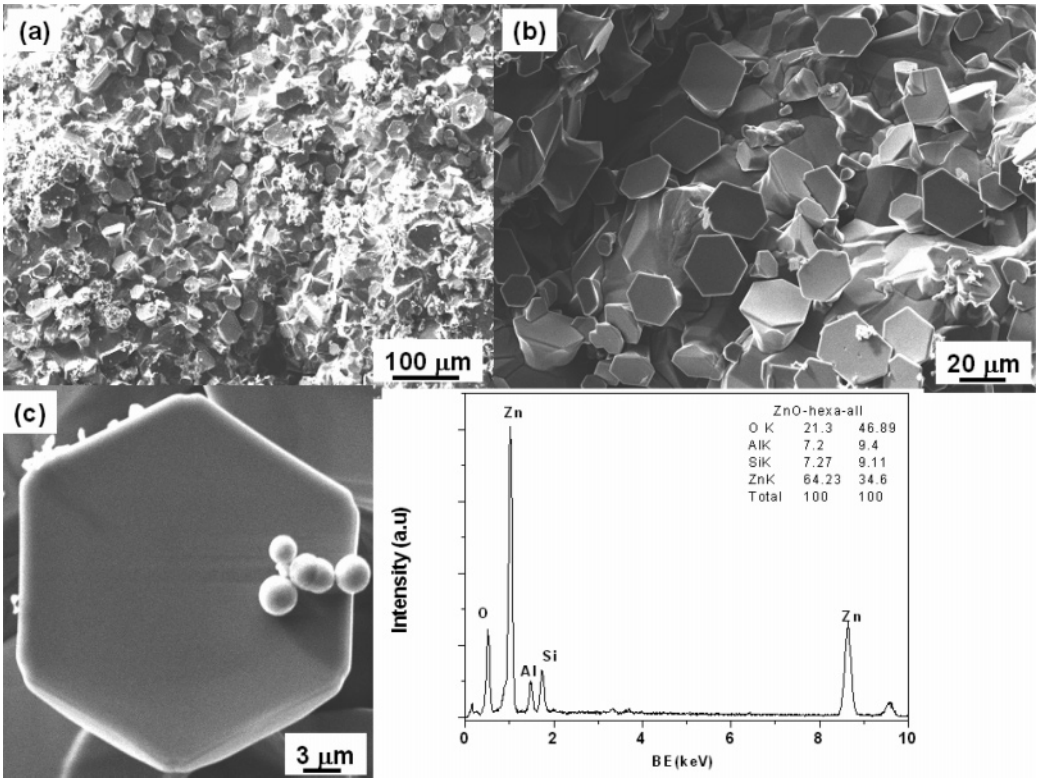

Figure 2. SEM images of the as-grown ZnO microhexagonal cones with different magnifications (a), (b), and (c), and the elemental composition as obtained from EDX recorded for hexagonal cones (d).

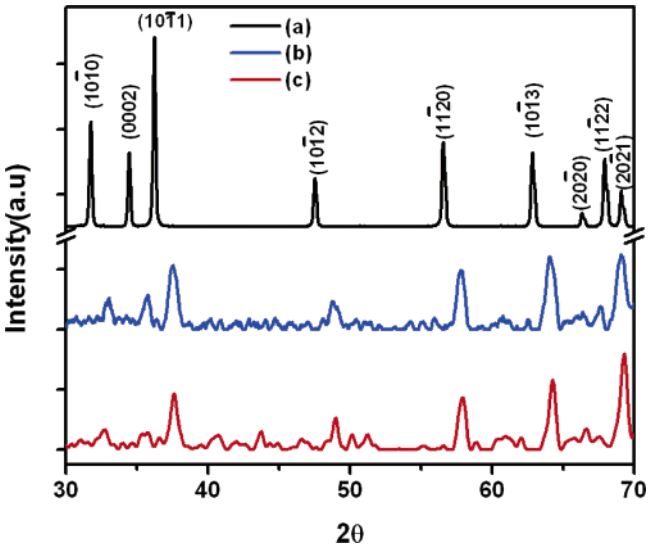

Figure 3. XRD patterns of (a) commercial ZnO (Aldrich 99.99%), (b) micropencils, and (c) microhexagonal cones.

To understand the oxidation state of both the structures and to compare their growth kinetics, analysis of the change in electronic state of the material is of particular significance. Accordingly, XPS analysis has been carried out on all samples. Consequently, Figure 4 shows the deconvulated C1s peak for commercial ZnO and freshly prepared micropencils and microhexagonal structures. In all XP spectra, the hollow circles denote the original data and solid lines represent the fitted curves and the deconvoluted individual peaks of different species present in the sample. All binding energy positions of the elements are listed in Table 1. For commercial ZnO, micropencils and hexagonal structures, the peaks at binding energy of 285 eV can be attributed to the C1s, while the peaks at binding energies of 287.8, 287.6, and 287.1 eV could be attributed to the adsorbed carbon species.

TABLE 1: All the Binding Energy Positions of the Element Present in Different ZnO Structures[a]

		BE (eV)		
species	chemical species	ZnO− Aldrich	microhexagonal cones	micropencils
C	1s	285	285	285
	adsorbed	287.8	287.6	287.1
Zn	$2P_{1/2}$	1044.7	1047.5	1045.4
	$2P_{3/2}$	1021.7	1024.5	1022.3
O	1s	530.2	530.2	530.6
	adsorbed	531.8	533.1.7	532.3
	lattice oxygen of ZnO_x/SiO_x		535.1	533.9
Si	$2P_{3/2}$			102.8
	$2P_{1/2}$		105.1	

[a] The spectra were fitted using a combined polynomial and Shirley type background function.

Figure 5 shows the deconvulated O1s peak for all the ZnO structures under investigation. For commercial ZnO the peak at binding energy of 530.2 eV can be attributed to the O1s, while the peak at binding energy of 531.8 eV is attributed to the adsorbed oxygen species. In case of micropencils and hexagonal cones, the oxygen peak can be deconvulated in three different peaks corresponding to O1s, adsorbed oxygen, and lattice oxygen of ZnO_x/SiO_x respectively.

Figure 6 shows the spectra for Zn signals for all samples. Interestingly, for both the micropencils and the hexagonal structures the two peaks corresponding to the Zn $2p_{1/2}$ and Zn $2p_{3/2}$ signals are found to be shifted toward the higher binding energy side and could be attributed to the incorporation of Si into the ZnO matrix. Using the atomic sensitivity factors, the

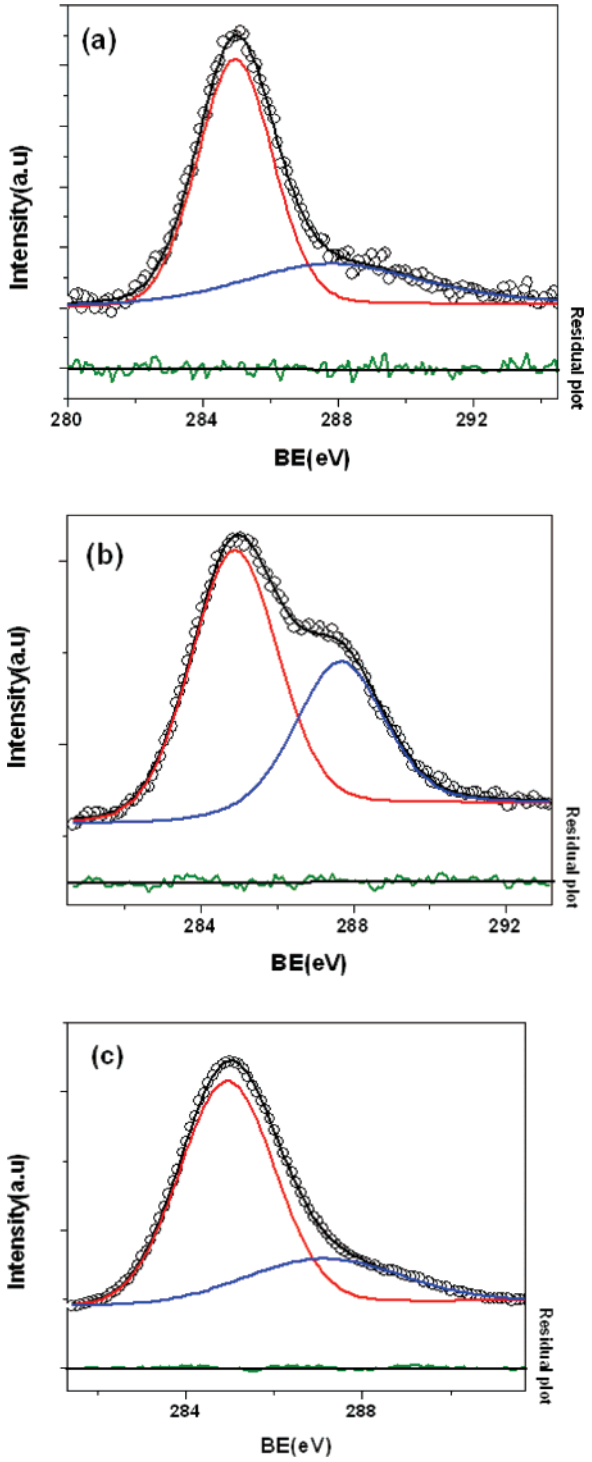

Figure 4. Deconvoluted C1s XPS peak for (a) commercial ZnO (Aldrich 99.99%), (b) micropencils, and (c) microhexagonal cones.

ratio of Zn:O is calculated using the relation

$$\mathrm{Zn}(2p_{3/2})/\mathrm{O1s} = I_{\mathrm{Zn}}/I_{\mathrm{O}} \times \sigma_{\mathrm{o}}/\sigma_{\mathrm{Zn}} \times (\mathrm{KE}_{\mathrm{Zn}}/\mathrm{KE}_{\mathrm{O}})^{1/2} \quad (1)$$

where I_{Zn} is the area under the curve of deconvoluted $\mathrm{Zn}(2p_{3/2})$, I_{O} is the area under the curve of deconvoluted $\mathrm{Zn}(2p_{1/2})$, σ_{o} and σ_{Zn} are the atomic sensitivity factors for O (2.85) and Zn (9.29), respectively, and $\mathrm{KE}_{\mathrm{Zn}}$ and KE_{O} are the kinetic energies of the electron of Zn and O, respectively. The ratio of Zn:O varies from 1:1.01 for commercial ZnO, 1: 0.3 for micropencils to 1: 1.1 for hexagonal cones.

Figure 7 shows the spectra for Si signals for both the micropencil and microhexagonal structures, respectively. Interestingly, for ZnO pencils a peak at binding energy of 102.8 eV is observed, which could be attributed to the signal from Si^{2+} ($2P_{3/2}$, SiO). However, in the case of microhexagonal cones the signal at the BE of 105.1 eV could be attributed to the Si^{4+} ($2P_{1/2}$, SiO_2).[12] The appearance of Si peaks further suggests that Si acts as a nucleating aid and probably gets incorporated into the ZnO matrix.

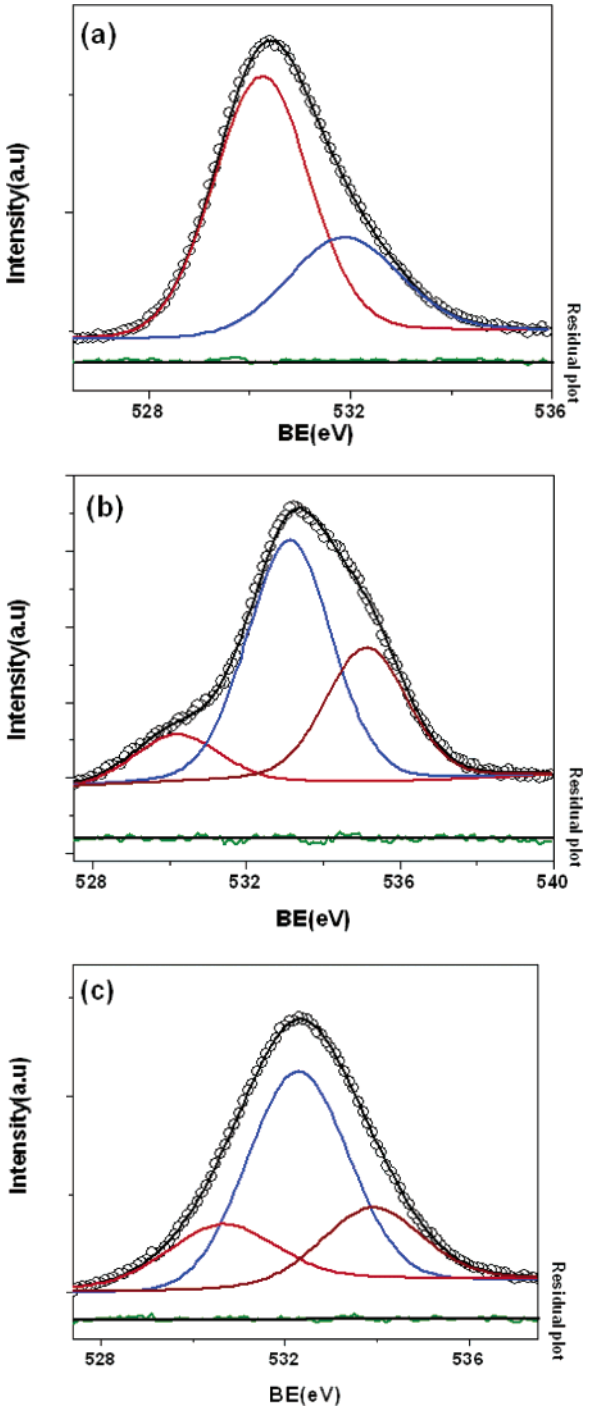

Figure 5. Deconvoluted O1s XPS peak for commercial ZnO (Aldrich 99.99%), (b) micropencils, and (c) microhexagonal cones.

(b) Plausible Growth Mechanism. To understand the growth kinetics, the TG-DT analysis of the Zn metal was performed under similar environment used for the synthesis of these remarkable ZnO microstructures (Figure 8). Up to 300 °C, a weight loss of 1.08 wt % attributed to the evaporation of impurities such as adsorbed moisture is observed. With a further increase in temperature up to 650 °C, the observed weight loss

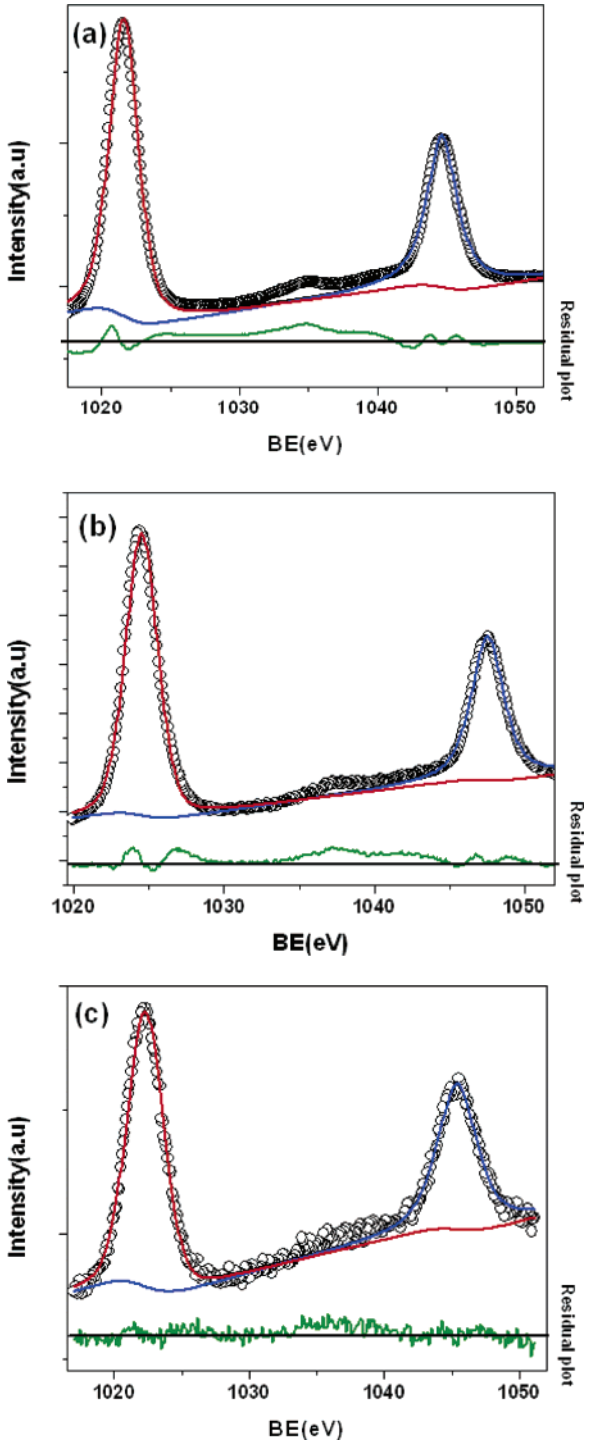

Figure 6. Deconvoluted Zn 2P XPS peaks for (a) commercial ZnO (Aldrich 99.99%), (b) micropencils, and (c) microhexagonal cones.

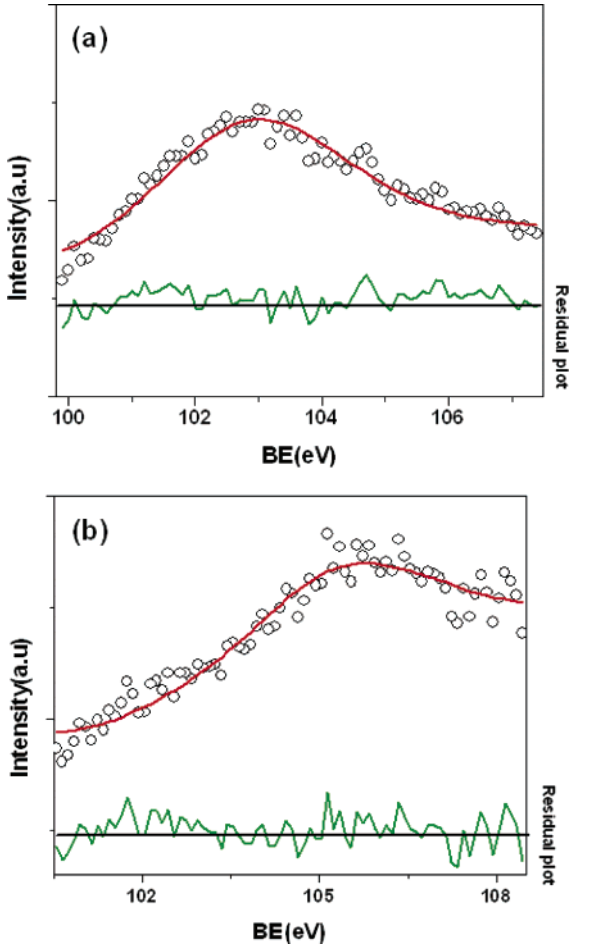

Figure 7. Deconvoluted Si XPS peak corresponding to (a) Si^{2+} ($2P_{3/2}$, SiO) in micropencils and (b) Si^{4+} ($2P_{1/2}$, SiO_2) peaks in microhexagonal cones.

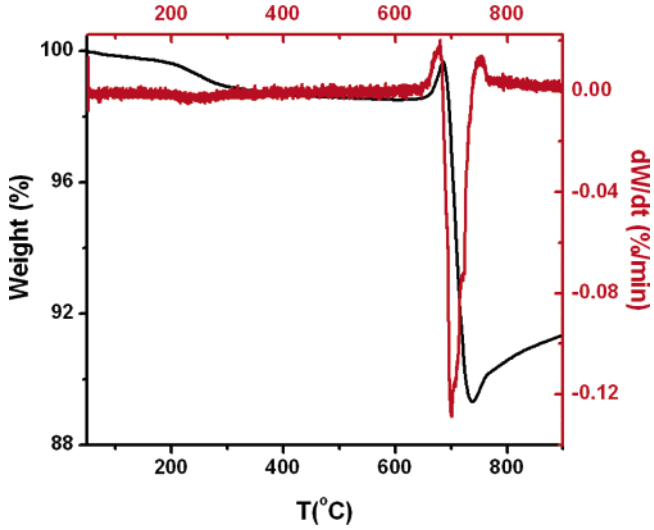

Figure 8. TG-DTA curve of the Zn metal under similar environment used for the synthesis of ZnO microstructures.

of 1.4% could be attributed to the slow evaporation of Zn. However, from 650 °C to 730 °C, a small weight gain (0.94 wt %) due to the conversion of Zn to ZnO species is seen. On the contrary, above 730 °C, a sharp loss of about 10.3 wt % is seen, which could be assigned to the evaporation of Zn species. At this temperature Zn metal gets transformed into a liquid droplet, and with a further increase in temperature, a weight gain of about 2 wt % observed subsequently could be attributed to the conversion of Zn species to ZnO. Thus, with the increase in the temperature, Zn metal transforms into liquid droplets with a small loss of Zn species, and this liquid droplet subsequently grows into a ZnO layer consisting of large grains on which several nucleating sites are generated. On this site several ZnO nuclei selectively grow along the crystallographic orientation of ZnO grain due to the strong epitaxial relation between them.[13] Continuous feeding of Zn vapor and oxygen into favorable nucleating sites will lead to vertical growth of ZnO structures possessing the same direction of *c*-plane to the ZnO grain as per the vapor−liquid−solid progression.

Further, EDX carried out on the substrate used (refractory brick) (Figure 9a) implies that it mainly consists of Si and Al.

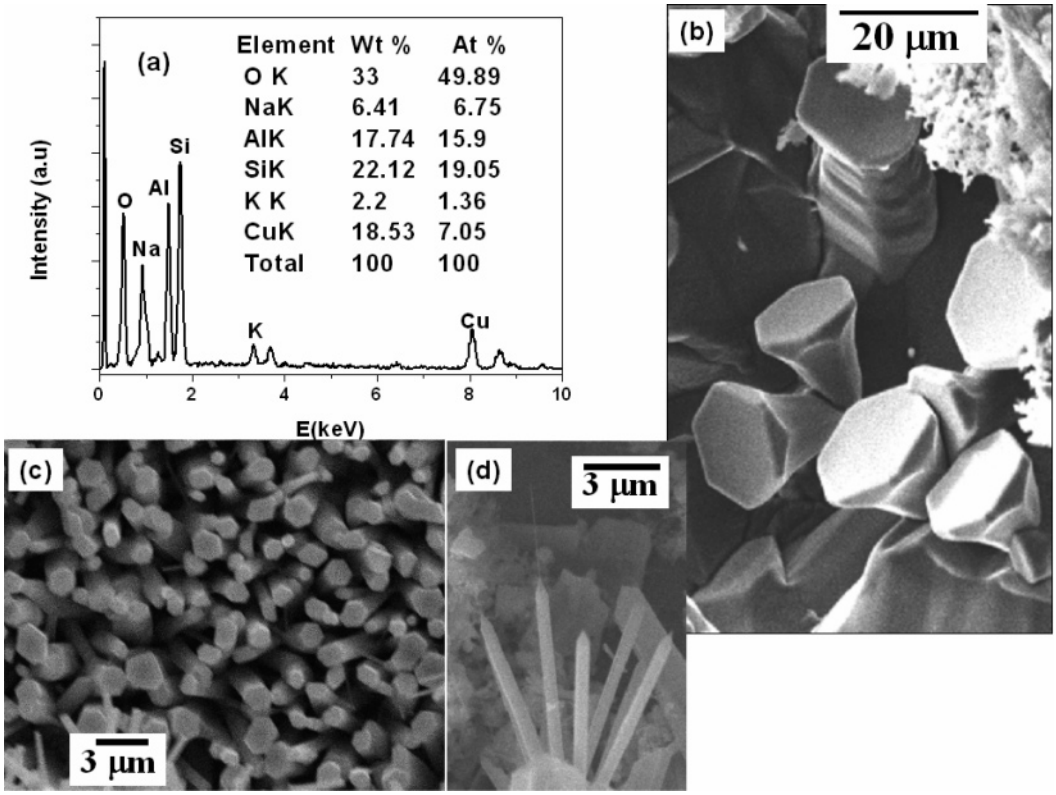

Figure 9. (a) EDX of the aluminosilicate refractory brick substrate used, (b) SEM image suggesting that the shank of the hexagonal cones originates from the substrates, and (c) hexagonal cones emerging out of the Si-wafer, when the experiments were carried out in similar conditions and (d) narrow pen tips on micropencils.

Among these, Si in the form of SiO_2 is expected to contribute to the microstructural growth. Surprisingly, when the experiments were carried out under similar conditions with Si−(100) wafer instead of aluminosilicate substrate, large number of hexagonal cones are seen originating from the substrate (Figure 9b). Recently, Ajayan et al. have reported the selective growth of oriented CNTs on patterned SiO_2 on Si(100) substrates.[14] They have observed that although there is no nanotube growth on silicon, aligned nanotubes grow readily on SiO_2 in a direction that is normal to the substrate surface. Similarly, in the present case, the shanks of the hexagonal cones originate from the substrate (Figure 9c), probably from the sites containing the Si species. Moreover, the hexagonal cones resemble the micropyramids synthesized via strong electrostatic interactions between the ions in the melt (solvent) and the polar surfaces of ZnO.[15] During the crystal growth, the polar surfaces usually appear as growing surfaces because of their higher surface energy, exhibiting small facets even disappearing during the crystal growth. For example, in ZnO growth, the highest growth rate is usually along the *c*-axis and the large facets are usually $\{01\bar{1}0\}$ and $\{2\bar{1}\bar{1}0\}$ nonpolar surfaces, rather than the polar $\{000\bar{1}\}$ surfaces. In contrast to the nonpolar surfaces, the polar $\{10\bar{1}1\}$ planes have a higher surface energy and usually grow too fast to be seen in the final shape of the crystal.[16] Further, some of the pencil structures also exhibit a narrow pen tips on the top (Figure 9d). Such structures have also been reported during cooling, owing to continuously decreasing zinc vapor pressure with decreasing temperature.[17] Moreover, the nucleation size of the pen tips is determined by the size of the platform area of the micropencil structures. Interestingly, when additional experiments were performed using alumina substrates instead of Si-wafer, multipod structures were observed.[18] This further signifies that the presence of Si species is crucial in governing the morphology of ZnO structures.

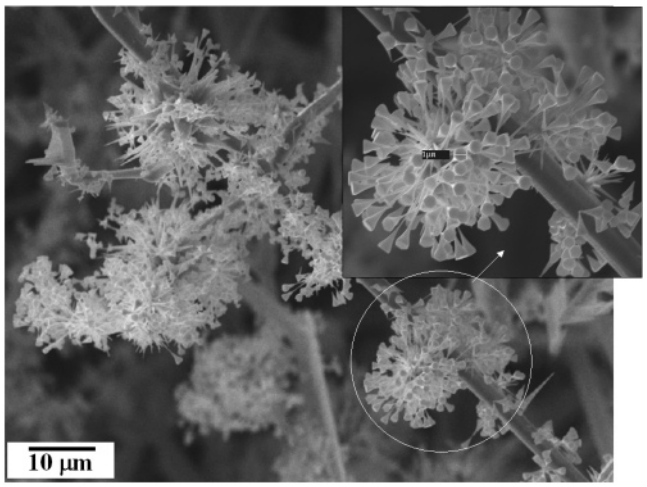

Figure 10. SEM image of a novel flower-like geometry also observed on the substrate at lower temperature between 200 and 500 °C.

Remarkably, a unique flower-like geometry is also observed on aluminosilicate substrates at lower temperature between 200 and 500 °C, as shown in Figure 10. These structures are found to grow on a central microwire, like a tree with flowers. The flower consists of large number of nanowires originating from a single point with tapering end possessing a hexagonal structure on the tip. Some of the hexagonal structures are observed to be separate from the flower suggesting the growth of nanowires to be one of the prominent phenomena. The different length of the nanowires implies various stages of incomplete growth. Indeed, the structure resembles to the needles reported by Wang et al.[19] with bigger dimensions. In our case, we speculate that the metallic Zn droplets are carried away to the substrate wherein the Si species present on the substrate acts as a nucleating site to grow ZnO microstructures. Moreover, during the growth

process the polar planes possessing the high surface energy grow faster to give the final morphology. However, when the arms of the wires grow sufficiently long, due to the strain induced in them, the hexagonal cones detach (Figure 10) from the central wire leading to the formation of sharp needle-like structures. For substrates kept at the middle of the furnace (950 °C), the growth process is faster because of the high temperature following a vapor−liquid−solid progression. While for the substrates kept at the lower temperature zone, the growth process is in the initial stages and hence only the hexagonal cones are observed. Further, some of the Zn vapor, evaporated from the starting material at a high temperature zone, flows and directly gets deposited on substrates at a low temperature region. At low temperature region the Zn vapors would be oxidized forming suboxides that could probably be assigned to the geometry of the substrate, which limits the amount of oxygen contributing to the reaction. Subsequently, suboxide forms liquid droplets, which in turn enhance the absorption and diffusion of Zn oxides during growth. Thus, the growth of hexagonal cones takes place via a two-step process. First as per the vapor−solid mechanism where the Zn vapor at high temperature flows to low temperature and reacts with oxygen to form suboxide. Second, these suboxides form liquid droplets, providing further nucleating sites along with SiO_2 for the formation of hexagonal cones and could be assigned to a vapor−liquid−solid mechanism.

Conclusions

In summary, the shape selective synthesis of two different morphologies of ZnO, namely micropencils and microhexagonal cones, has been successfully demonstrated using a simple approach of modified vapor deposition. XPS studies indicate that the BE of Zn species shifts to higher BE side, which could be attributed to the Si present in the matrix. Si species get incorporated into the ZnO matrix in Si^{2+}(SiO) and Si^{4+}(SiO_2) forms, which plays crucial role in deciding the morphology. Further, a plausible growth mechanism based on the results of SEM, XRD, XPS, and TGA has been proposed. It has been demonstrated that the micropencil grows via a vapor−liquid−solid progression while the microhexagonal cones grow in two steps following vapor−solid and vapor−liquid−solid mechanisms, respectively. These results are believed to be important for controlling the growth of ZnO structures realizing their simultaneous, multidirectional growth on templates of SiO_2 for various device applications.

Acknowledgment. N.S.R. thanks the Council of Scientific and Industrial Research (CSIR), New Delhi for the grant of a senior research fellowship. Authors are grateful to Dr. S. R. Sainker, Dr. A. B. Gaikwad and Dr. K. R. Patil for their help in characterization.

References and Notes

(1) Wang, Y.; Jiang, X.; Xia, Y. *J. Am. Chem. Soc.* **2003**, *125*(52), 16176.
(2) Wu, J.-M.; Shih H. C.; Wu, W.-T. *Chem. Phys. Lett.* **2003**, *413*, 490.
(3) Li, X.-L.; Lou, T.-J.; Sun, X.-M.; Li, Y.-D. *Inorg. Chem.* **2004**, *43*(17), 5442.
(4) (a) Kong, X. Y.; Ding, Y.; Yang, R. S.; Wang, Z. L. *Science* **2004**, *303*, 1348. (b) Wang, Z. L.; Kong, X. Y.; Zuo, J. M. *Phys. Rev. Lett.* **2003**, *91*, 185502. (c) Bai, X.; Wang, E. G.; Gao, P.; Wang, Z. L. *Nano Lett.* **2003**, *3*(8), 1147. (d) Dai, Z. R.; Pan, Z. W.; Wang, Z. L. *Adv. Funct. Mater.* **2003**, *13*, 9.
(5) Xu, N. S.; Huq, S. E. *Mater. Sci. Eng.* **2005**, *48*, 47.
(6) Roy, V. A. L.; Djurišić, A. B.; Chan, W. K.; Gao, J.; Lui, H. F.; Surya, C. *Appl. Phys. Lett.* **2003**, *83*, 141.
(7) (a) Zhu, Z.; Chen, T.-L.; Gu, Y.; Warren, J.; Osgood, R. M., Jr. *Chem. Mater.* **2005**, *17*(16), 4227. (b) Lyu, S. C.; Zhang, Y.; Lee, C. J.; Ruh, H.; Lee, H. J. *Chem. Mater.* **2003**, *15*(17), 3294.
(8) Yan, H.; He, R.; Pham, J.; Yang, P. *Adv. Mater.* **2003**, *15*, 402.
(9) Gao, P. X.; Wang, Z. L. *Small* **2005**, *1*, 945.
(10) (a) Ramgir, N. S.; Mulla, I. S.; Vijayamohanan, K. P. *J. Phys. Chem. B* **2004**, *108*, 14815. (b) Ramgir, N. S.; Mulla, I. S.; Vijayamohanan, K. P. *J. Phys. Chem. B.* **2005**, *109*(25), 12297.
(11) Yin, M.; Gu, Y.; Kuskovsky, I.; Andelman, T.; Zhu, Y.; Neumark, G. F.; O'Brien, S. *J. Am. Chem. Soc.* **2004**, *126*, 6206.
(12) Chen, T. P.; Liu, Y.; Sun, C. Q.; Tse, M. S.; Hsieh, J. H.; Fu, Y. Q.; Liu, Y. C.; Fung, S. *J. Phys. Chem. B* **2004**, *108*(43), 16609.
(13) Jeong, J. S.; Lee, J. Y.; Cho, J. H.; Suh, H. J.; Lee, C. J. *Chem. Mater.* **2005**, *17*, 2752.
(14) Wei, B. Q.; Vajtai, R.; Jung, Y.; Ward, J.; Zhang, R. Ramanath, G.; Ajayan, P. M. *Nature* **2002**, *416*, 495.
(15) Zhou, X.; Xie, Z.-X.; Jiang, Z.-Y.; Kuang, Q.; Zhang, S.-H.; Xu, T.; Huang, R.-B.; Zheng, L.-S. *Chem. Commun.* **2005**, *44*, 5572.
(16) Li, W.-J.; Shi, E.-W.; Zhong, W.-Z.; Yin, Z.-W. *J. Crys. Growth* **1999**, *203*, 186.
(17) Wang, R. C.; Liu, C. P.; Huang, J. L.; Chen, S.-J.; Tseng, Y.-K.; Kung, S.-C. *Appl. Phys. Lett.* **2005**, *87*, 013110.
(18) Ramgir, N. S.; Mulla, I. S.; Pillai, K. P.; Late, D. J.; Bhise, A. B.; More, M. A.; Joag, D. S. *Appl. Phys. Lett.* **2006**, *88*(3), 042107.
(19) Yao, B. D.; Chan, Y. F.; Wang, N. *Appl. Phys. Lett.* **2002**, *81*, 757.